Enhancing thermal degradation stability of $BaSi_2O_2N_2:Eu^{2+}$ for white light-emitting diodes by ultra-thin Al_2O_3 layer via atomic layer deposition

Zhao, Yujie; Wang, Xiao; Li, Quan an; Zhang, Xinyu; Li, Ye; Xie, Rong Jun; van Ommen, J. Ruud; Hintzen, H. T.

DOI
10.1016/j.ceramint.2023.06.013

Publication date
2023

Document Version
Final published version

Published in
Ceramics International

Ceramics International 49 (2023) 27423–27429

Contents lists available at ScienceDirect

Ceramics International

journal homepage: www.elsevier.com/locate/ceramint

Enhancing thermal degradation stability of $BaSi_2O_2N_2:Eu^{2+}$ for white light-emitting diodes by ultra-thin Al_2O_3 layer *via* atomic layer deposition

Yujie Zhao [a,b,c], Xiao Wang [a], Quan-an Li [a], Xinyu Zhang [b], Ye Li [b], Rong-Jun Xie [b,*], J. Ruud van Ommen [c], H.T. Hintzen [d,**]

[a] College of Materials Science and Engineering, Henan University of Science and Technology, Luoyang, 471000, PR China
[b] Fujian Key Laboratory of Surface and Interface Engineering for High Performance Materials, College of Materials, Xiamen University, Xiamen, 361005, PR China
[c] Department of Chemical Engineering, Faculty of Applied Sciences, Delft University of Technology, 2629, HZ Delft, the Netherlands
[d] Fundamental Aspects of Materials and Energy, Faculty of Applied Sciences, Delft University of Technology, 2629, HZ Delft, the Netherlands

ARTICLE INFO

Handling Editor: Dr P. Vincenzini

Keywords:
Phosphor
wLED
Thermal stability
Atomic layer deposition

ABSTRACT

The cyan-emitting $BaSi_2O_2N_2:Eu^{2+}$ phosphor is a promising narrow-band and high-efficiency luminescent material used in wide-color-gamut white light-emitting diodes (wLEDs). However, its serious degradation under thermal attacks hinders its practical applications and needs to be improved. Herein, we proposed to deposit a nano-sized Al_2O_3 film around each $BaSi_2O_2N_2:Eu^{2+}$ particle through atomic layer deposition (ALD) in a fluidized bed reactor to improve its thermal stability. Thermal gravimetric analysis results showed that the Al_2O_3 layer with a thickness of only 11 nm had an obvious anti-oxidization effect, by which the oxidation temperature in air of the Al_2O_3 coated phosphor was largely increased from ~550 to ~750 °C. Moreover, the Al_2O_3 coated phosphor remained 93% of its luminescence intensity in comparison to 73% of the uncoated one when degraded under water-steam at 200 °C for 24 h. The oxidization of both the $BaSi_2O_2N_2$ host matrix and the doped Eu^{2+} ions was reduced by the Al_2O_3 layer. Meanwhile, the wLEDs fabricated with the Al_2O_3 coated phosphor showed a luminous flux of 3 times higher than that of the uncoated one when aged under 100 mA for 300 h. The greatly improved thermal degradation property of $BaSi_2O_2N_2:Eu^{2+}$ phosphor and the reliability of the wLEDs indicate that the ALD approach could be a feasible route to produce uniform and nano layers on phosphors and enhance their stability.

1. Introduction

Phosphors play an irreplaceable role in energy-saving wLEDs [1–3]. Generally, phosphors applied to wLEDs need to have high quantum efficiency, suitable excitation and emission spectra, and good thermal quenching properties [4–6]. Besides, the phosphors should be robust under thermal, moisture, and irradiation attacks [7–11].

Eu^{2+}-doped $MSi_2O_2N_2$ (M = Ca, Sr, Ba) phosphors show excellent photoluminescence properties and good chemical stabilities [12–14]. They emit visible light from cyan to yellow depending on the species of alkaline earth metals and dopants [15–17]. Among them, $BaSi_2O_2N_2:Eu^{2+}$ (BSON) has a narrow-band cyan emission, a full-width at half maximum (FWHM) of only ~40 nm, and high quantum efficiency of ~85%, which can be used to fabricate super-high color rendering wLEDs [18–20]. However, BSON shows obvious thermal degradation under air or moisture attacks. Different from thermal quenching, thermal degradation of BSON is an irreversible deformation, which makes it hard to be practically used in wLEDs with high reliability and longevity.

Many efforts have been devoted to investigating the thermal degradation mechanisms and reliability of $MSi_2O_2N_2$ phosphors [21,22]. Wang et al. found that the photoluminescence intensity of the $SrSi_2O_2N_2:Eu^{2+}$ (SSON) phosphor decreased when baked at 200–600 °C in air, which is mainly due to the oxidation of Eu^{2+} induced by its layered structure [23]. At the same time, $SrSiO_3$ was formed on its surface due to the oxidation of the host lattice. The oxidation of both the host lattice and the activator decreases the luminous intensity of SSON. Zhang et al. observed that the deterioration of SSON was mainly caused by the oxidation of the host lattice when calcined at 400 °C in air [24].

As to BSON, it has a similar layered structure as SSON, yet the coordination environment of Ba is different from Sr [15]. Therefore, the

* Corresponding author.
** Corresponding author.
E-mail addresses: rjxie@xmu.edu.cn (R.-J. Xie), H.T.Hintzen@tudelft.nl (H.T. Hintzen).

https://doi.org/10.1016/j.ceramint.2023.06.013
Received 25 April 2023; Received in revised form 28 May 2023; Accepted 2 June 2023
Available online 5 June 2023

BSON phosphor also has the problem of thermal degradation that needs to be solved [25–27]. Wu et al. found that the thermal quenching and thermal cycling degradation of BSON caused by the oxidation of Eu^{2+} were reduced by 11.4% and 6.1% through SiC doping in the lattice, respectively [28]. Zhang et al. reported that the thermal quenching stability at 150 °C was increased by 2.4% and the thermal degradation after being calcinated at 500 °C was decreased by 15% when a SiO_2 coating was applied on BSON [29]. Generally, coating a protective layer on the phosphor surface is a feasible approach to improve its stability. However, due to the rather high SiO_2 coating thickness, the emission loss is quite significant, and there is still much room left to improve the thermal stability of BSON phosphor by applying a much thinner but nevertheless closed coating.

Atomic layer deposition is a gas phase deposition technique that has been applied to deposit passivated layers in many areas for superiorly stable materials [30,31]. In our previous work, a uniform Al_2O_3 thin layer was deposited on the $Sr_2Si_5N_8:Eu^{2+}$ phosphor surface by using ALD in a fluidized bed reactor (FB-ALD), and the relative photoluminescence intensity of the coated phosphor after degraded under 200 °C in air for 2 h was improved from 80% to 95% in comparison to the uncoated one [32]. Based on cyclic self-limiting reactions, ALD allows controlling the thickness of the Al_2O_3 layer down to atomic levels with high uniformity and conformity [33,34]. In this work, we attempted to enhance the thermal degradation stability of BSON by coating an ultra-thin Al_2O_3 layer on the phosphor surface. The influence of the Al_2O_3 layer on the photoluminescence property and thermal stability of BSON, as well as on the reliability of the fabricated LED devices was investigated.

2. Experimental section

2.1. Starting materials

The $BaSi_2O_2N_2:Eu^{2+}$ phosphor powders were purchased from Beijing Nakamura Yuji Science and Technology Co. Ltd. Trimethylaluminium (TMA, select semiconductor grade) supplied by Akzo-Nobel HPMO (Amersfoort, The Netherlands) was used as Al-precursor, and O_3 was chosen as the oxidizer. High-purity nitrogen gas (grade 5.0) with a flow rate of 1 L/min was provided as the carrier gas to introduce the Al-precursor and oxidizer into the reactor and purge the system.

2.2. Al_2O_3 ALD in a fluidized bed reactor

The ALD of Al_2O_3 was carried out using a home-built FB-ALD system reported in our previous work [32]. During the deposition process, 4g BSON phosphor powders were filled into a glass column which was placed on a single motor Paja PTL 40/40-24 vibration table to assist the fluidization. A controllable infrared lamp parallel to the column was used to adjust the temperature of the reactor chamber. The reactor was kept at atmospheric pressure and the deposition temperature was set at 100 °C. The feeding sequence is TMA - N_2 - O_3 – N_2 with a dosing time of 60 s–240 s - 60 s–240 s, and the number of the coating cycles was set as 5, 10, and 20, respectively.

2.3. Characterizations

An X-ray diffractometer (XRD, Bruker D4 Endeavor, Germany) was used to examine the phase composition of the phosphor. Scanning electron microscopy (SEM, TM3000, Hitachi, Japan) and particle size analysis by laser diffraction (LS-POP(6), OMEC, China) were employed to study the morphology and particle size of the phosphor. Transmission electron microscopy (TEM, JEOL JEM2100, Japan) operating at a voltage of 200 kV was used to observe the coating layer. X-ray photoelectron spectroscopy (XPS) analysis was obtained from a Thermo Scientific K-Alpha + spectrometer (Thermo Fisher Scientific, USA) equipped with an Al Kα monochromated X-ray source. The photoluminescence spectra were collected using a fluorescence spectrometer (F-4600, Hitachi, Japan). The quantum efficiency was measured on a fluorescence spectrophotometer (FLS980, Edinburgh Instrument, UK) equipped with visible photomultiplier tube detectors (Hamamatsu R982P, Japan). The UV–Vis diffuse reflection spectra were measured on a UV-3600 Plus spectrometer (Shimadzu, Japan). A thermogravimetric analyzer (TGA/SDTA 851e Mettler Toledo, Switzerland) was used to study the thermal oxidation stability of the phosphor powders. The weight change of the samples in flowing air was recorded by heating them from 25 to 120 °C and holding for 10 min, then to 1000 °C and holding for 30 min at a heating rate of 10 °C/min.

2.4. Degradation of the samples

The moisture-assisted thermal degradation was done by loading 0.2 g of the phosphor powders into a flat-bottomed silica glass cell that was placed in a Teflon lining and immersed in 5 mL of distilled water. The Teflon lining was then enclosed by a stainless-steel reactor and heated to 200 °C for 24 h, followed by naturally cooling to room temperature. The degraded phosphor powders were dried in an oven at 60 °C for 12 h. The pH value of the surrounding water outside the silica glass was recorded by a pH meter (Cnoble, China).

2.5. Fabrication of LEDs

The BSON and Al_2O_3 coated BSON (BSON@Al_2O_3) phosphor powders were fabricated into LEDs by combining them with a blue InGaN LED chip, respectively. 0.1 g phosphor powder was mixed with 1.5 g organic resin and then mounted on the InGaN chip to fabricate cyan LEDs. The fabricated LEDs were naturally solidified overnight. The luminous flux and chromaticity coordinates of the fabricated LEDs driven at 100 mA for different times were measured by an ATA-500 auto-temperatured LED opto-electronic analyzer (EVERFINE Corporation, China).

3. Results and discussion

3.1. Characterizations of the coated phosphors

SEM images of BSON and BSON@Al_2O_3 are shown in Fig. 1a. It shows that the BSON particles are irregular and have a particle size of 5–20 μm. The median diameter (D_{50}) of the BSON particles is determined to be 8.5 μm. No obvious difference in the sample surface between the BSON and BSON@Al_2O_3 is observed since the coated transparent Al_2O_3 layer is conformal and ultra-thin as confirmed by TEM.

XRD patterns of BSON and BSON@Al_2O_3 with different numbers of coating cycles were examined to investigate the impact of the Al_2O_3 coating on the phase composition. As seen in Fig. 1b, the diffraction peaks of BSON are consistent with the standard card of $BaSi_2O_2N_2$ (PDF # 17-3758), and some diffraction peaks of $BaSi_6N_8O$ (PDF # 41-5472) are also detected as an impurity phase. Compared with BSON, no peak shifts or secondary phases were detected in BSON@Al_2O_3, indicating that the deposition process has no obvious influence on the phase or structure of the BSON phosphor. Diffraction peaks of crystalline Al_2O_3 are not detected in any of the BSON@Al_2O_3 samples, which is consistent with the literature reports that the Al_2O_3 layer deposited through ALD below 300 °C is generally amorphous [35].

The layer thickness of Al_2O_3 on the phosphor surface was observed by TEM. As can be seen in Fig. 2a, a nano-sized coating layer was successfully deposited on the surface of the phosphor particles. The Al_2O_3 layer is quite uniform and conformal, which has a narrow distribution of 4 ± 0.5, 6 ± 1, and 11 ± 1 nm for the samples coated with 5, 10, and 20 cycles, respectively. There is a linear relationship between the thickness of the Al_2O_3 layer and the number of coating cycles, demonstrating that the coating thickness can be well controlled by adjusting the number of coating cycles (Fig. 2b). One can also find that the growth rate of the

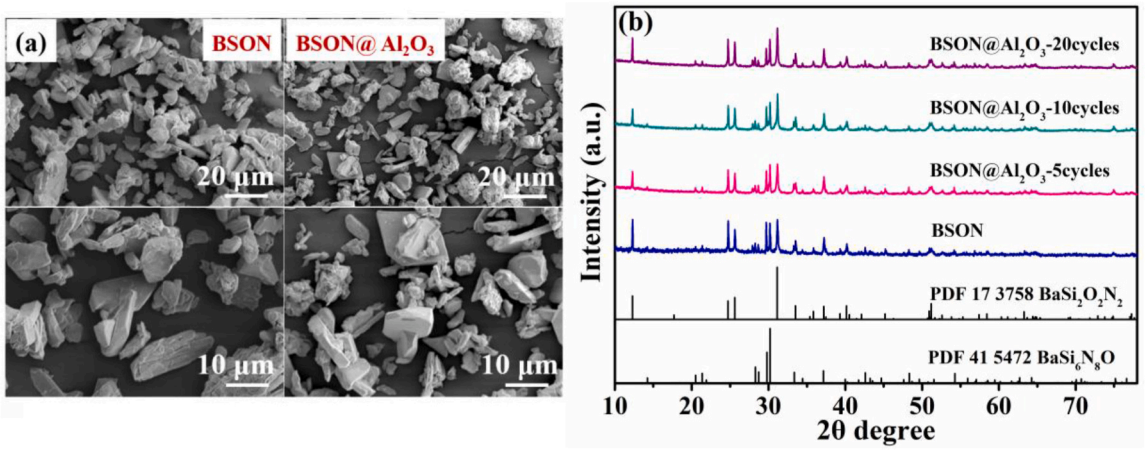

Fig. 1. SEM images (a) and XRD patterns (b) of the BSON and BSON@Al_2O_3 with different numbers of deposition cycles.

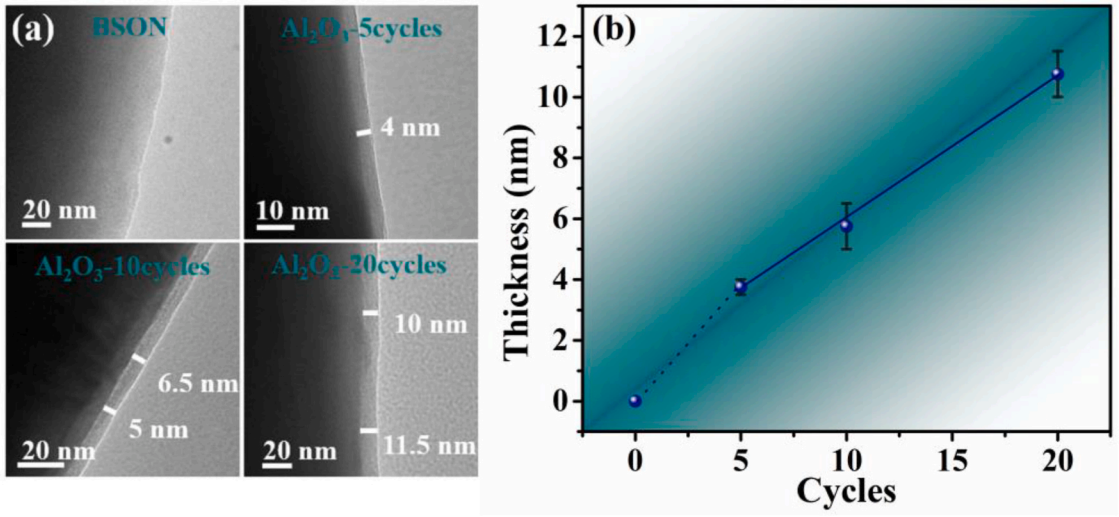

Fig. 2. (a) TEM images of BSON and BSON@Al_2O_3 with different numbers of coating cycles, and (b) the relationship between the coating thickness and the number of coating cycles. Gray vertical error bars indicate the TEM variation of the coating thickness.

Al_2O_3 layer is a little higher in the first 5 cycles, which may be due to the intrinsic substrate-enhanced growth nature of the ALD process [36,37]. In addition, the growth per cycle in the present work is calculated to be ~0.5 nm, which is larger than the reported one for ideal Al_2O_3 ALD (generally 0.1–0.2 nm), since the deposition of Al_2O_3 is affected by the working pressure, deposition temperature, reactor-type and so on [33].

To investigate the effect of the Al_2O_3 coating on the surface characteristics of the BSON phosphor, XPS analysis was carried out (Fig. 3). The Al signal at a binding energy of ~74.6 eV in the spectra of BSON@Al_2O_3 was detected while not in the spectra of uncoated BSON (Fig. 3b), which is in accordance with the Al–O bond and again demonstrates that the Al_2O_3 is successfully deposited on the surface of BSON particles [38,39]. Compared with the pristine BSON, the signal intensities of Ba and N elements decrease in the BSON@Al_2O_3 sample (Fig. 3c and d), which is ascribed to the signal block by the Al_2O_3 film. As expected, the signal intensity of O increases after the Al_2O_3 deposition (Fig. 3e). Moreover, the signal of Eu with a binding energy of ~1135.5 eV is detected in the BSON sample (Fig. 3f), which is assigned to Eu^{3+} that is already appeared on the surface of bare BSON particles [40,41]. The detectable intensity of Eu is also reduced in the BSON@Al_2O_3 sample due to the presence of the Al_2O_3 film.

3.2. Photoluminescence properties

The BSON and BSON@Al_2O_3 samples exhibit similar profiles of excitation and emission spectra (Fig. 4a and b), and the deposited Al_2O_3 film has no significant influence on the peak position of the BSON phosphor. The excitation and emission intensities decrease slightly after the Al_2O_3 coating, which is dependent on the number of the coating cycle (*i.e.* coating thickness). Moreover, the quantum efficiency (QE) of BSON@Al_2O_3 decreases slightly (Fig. 4c). The internal and external quantum efficiencies (IQE and EQE) of BSON@Al_2O_3 with various deposition cycles are decreased by 4–7% and 2–5%, respectively. This can be attributed to the following reasons, *i.e.*, (i) damage of the interface between BSON and Al_2O_3 by the highly reactive TMA and O_3 and the co-effect of the generated H_2O during the deposition process; (ii) the reduction of absorption of the incident photons at 275 nm (excitation wavelength) by the deposited Al_2O_3 layer, verified by the UV–Visible diffuse reflectance spectra (Fig. 4d).

3.3. Thermal degradation stability

The thermal stability of BSON and BSON@Al_2O_3 was studied by monitoring their thermal gravimetric plots in air atmosphere. As shown in Fig. 5a, the BSON@Al_2O_3 samples show an obvious weight loss as the

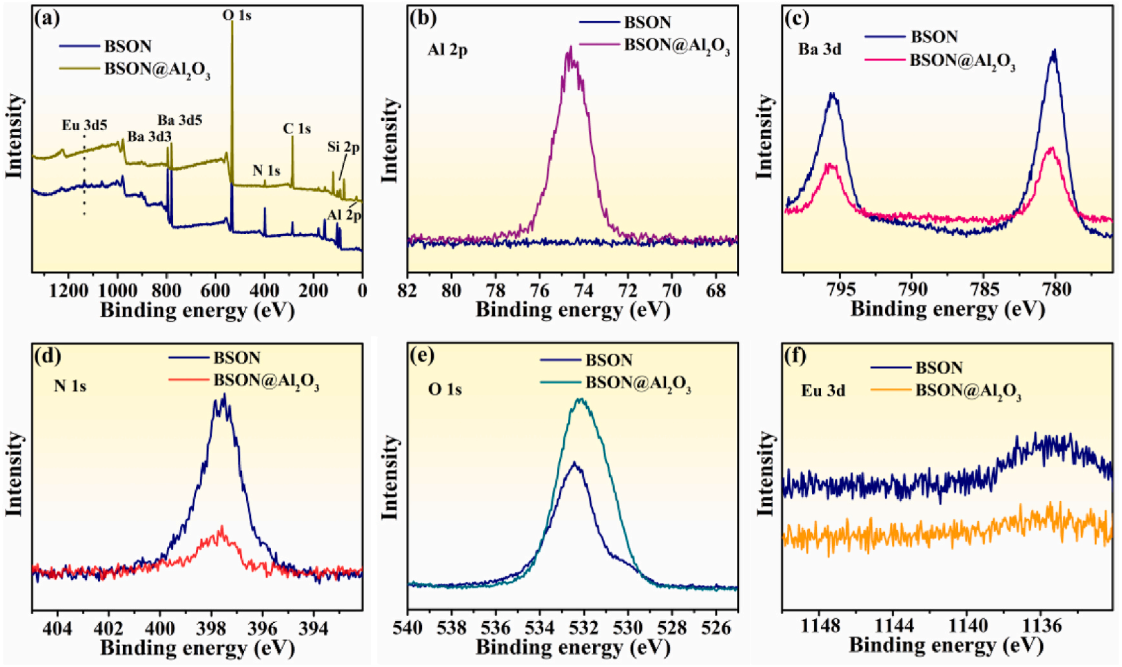

Fig. 3. XPS spectra of BSON and BSON@Al_2O_3 with a deposition number of 20 cycles.

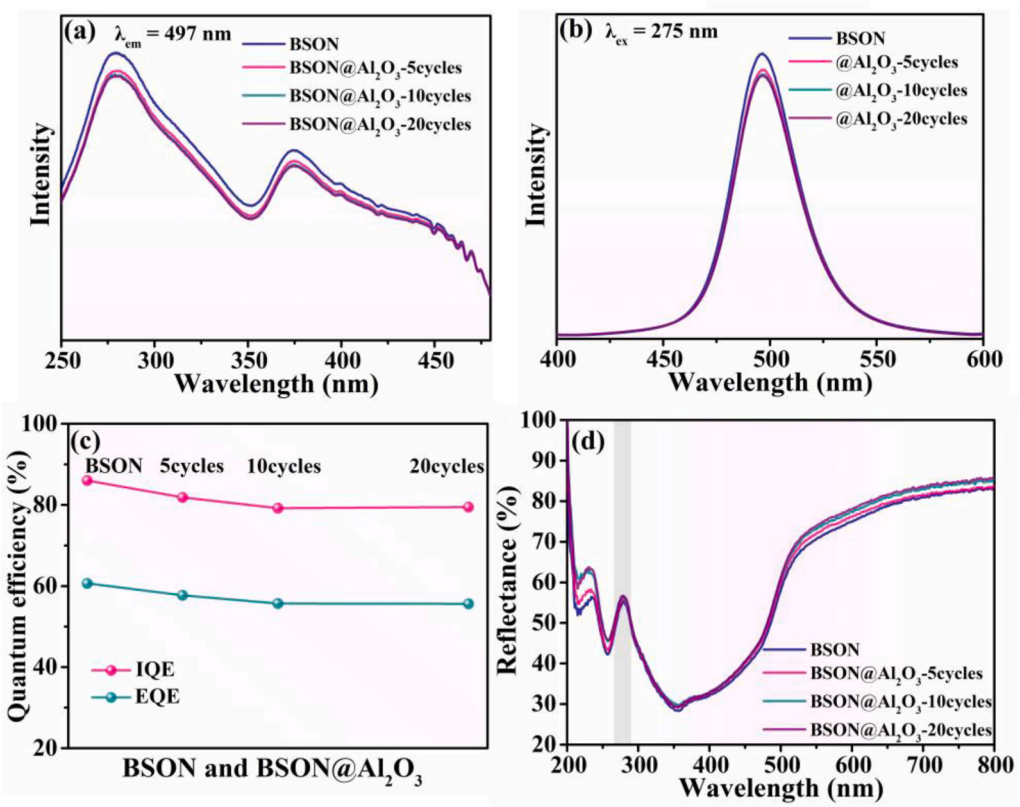

Fig. 4. Excitation spectra (a), Emission spectra (b), Quantum efficiency (c), and UV–Vis diffuse reflectance spectra (d) of BSON and BSON@Al_2O_3 with different numbers of deposition cycles.

temperature goes up to ~500 °C, which is ascribed to the desorption of water, hydroxyl groups, and carbon groups that are present in the Al_2O_3 layer [32,42,43]. A larger number of deposition cycles leads to a higher weight loss of the samples. Besides, the weight of the uncoated BSON particles starts to gain at ~550 °C and keeps rising at higher temperatures, indicating the oxidization of the host material. Compared with the uncoated BSON, BSON@Al_2O_3 shows a higher temperature at which the weight gain starts, which is ~630, ~695, and ~750 °C for the samples deposited with 5, 10, and 20 cycles, respectively. This signifies that the BSON@Al_2O_3 is well-protected by the Al_2O_3 layer against the

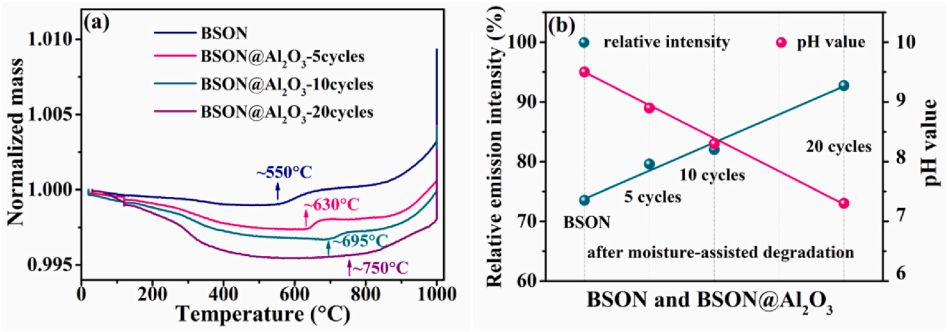

Fig. 5. (a) TGA curves of BSON and BSON@Al_2O_3, and (b) Relative emission intensity of BSON and BSON@Al_2O_3 and the pH values of the surrounding solutions after the moisture-assisted thermal degradation test.

thermal attack in air, thus its anti-oxidization property is then greatly improved.

In addition, the moisture-assisted thermal degradation of BSON and BSON@Al_2O_3 was conducted at 200 °C for 24 h. As seen in Fig. 5b, both phosphors show permanent loss in photoluminescence after degradation, but this loss is effectively reduced by the Al_2O_3 coating. The uncoated BSON losses as high as 27% of the luminescence intensity, whereas the BSON@Al_2O_3 with 20 deposition cycles losses only 7%. Therefore, the stability of the BSON phosphor under moisture-assisted thermal conditions can also be greatly enhanced by the Al_2O_3 coating. During the moisture-assisted thermal degradation test, ammonia gas is released and dissolved into the surrounding water owing to the decomposition of the BSON matrix, which will cause an increase of the pH value. After the degradation test, the pH value of the aqueous solution around the BSON particles is ~9.5, but it decreases to ~7.3 for the BSON@Al_2O_3 sample coated with 20 cycles of Al_2O_3 (Fig. 5b). It thus means that the moisture-assisted decomposition of the BSON phosphor is suppressed by the surface coating [44].

To reveal the moisture-assisted thermal degradation mechanism of BSON, SEM observation and XPS analysis were performed (Fig. 6). One can find that the surface of the uncoated BSON particles was destroyed and a lot of tiny particles appear after degradation, whereas it remains clear for the BSON@Al_2O_3 particles (Fig. 6a). The XPS spectra of the BSON and BSON@Al_2O_3 samples show that the signal intensity of O increases but that of N decreases after degradation, indicating the oxidation of the host. However, the changes in the signal intensities of O and N for the BSON@Al_2O_3 sample are much smaller than those of BSON, which implies that the Al_2O_3 layer well protects the phosphor against the moisture and thermal attacks. Moreover, XPS peaks of Eu 3d located at ~1125.5 and ~1156.5 eV are assigned to Eu^{2+}, but those of ~1135.5 and ~1164.4 eV are attributed to Eu^{3+}, respectively [24,40,41]. For the uncoated BSON, the signal intensity of Eu^{3+} is increased after degradation, indicating that the Eu^{2+} ions were partially oxidized to Eu^{3+}. It is difficult to identify the signal of Eu 3d in BSON@Al_2O_3 due to the shielding effect of the Al_2O_3 layer. Based on the above observations, the degradation mechanism of BSON and the protection effect by the Al_2O_3 thin layer are schematically shown in Fig. 6c.

3.4. LED aging tests

The BSON and BSON@Al_2O_3 powders were combined with a commercial 450 nm InGaN chip to fabricate cyan LEDs, respectively. As shown in Fig. 7a, the luminous flux of the cyan LEDs using uncoated BSON decreases severely from 17 to 3.8 lm after aging for 300 h, and only 22% of its initial value can be maintained. On the other hand, the luminous flux slowly decreases from 16.4 to 11.9 lm for the LEDs

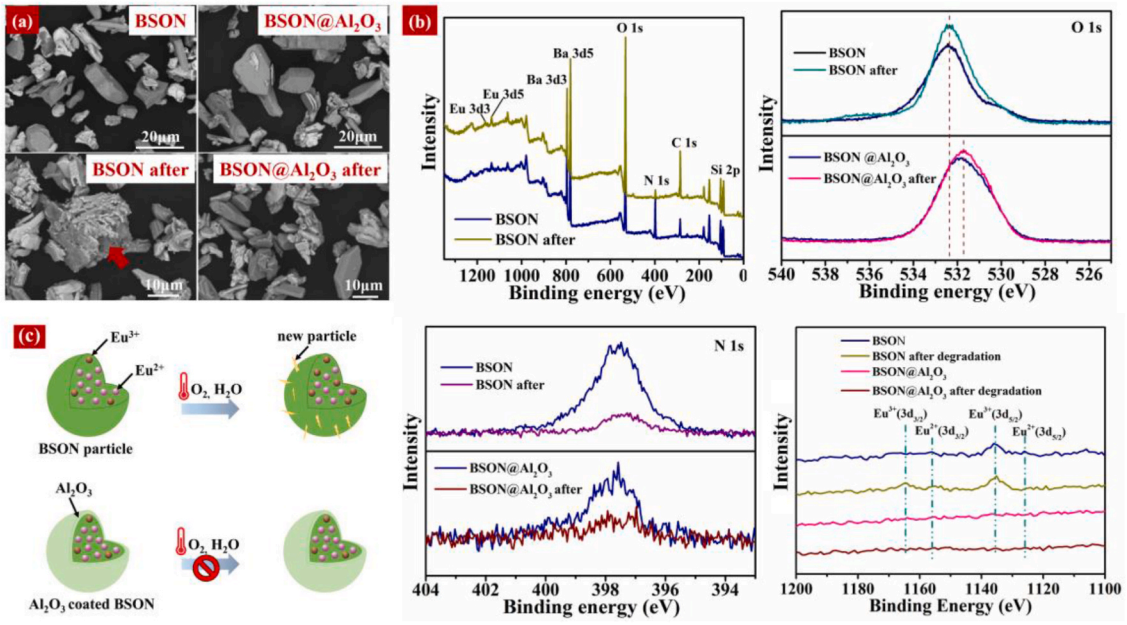

Fig. 6. (a) SEM images, (b) XPS spectra of BSON and BSON@Al_2O_3 deposited for 20 cycles before and after the moisture-assisted thermal degradation test, and (c) the schematic diagrams representing the degradation mechanism of BSON and the protective effect of the Al_2O_3 coating.

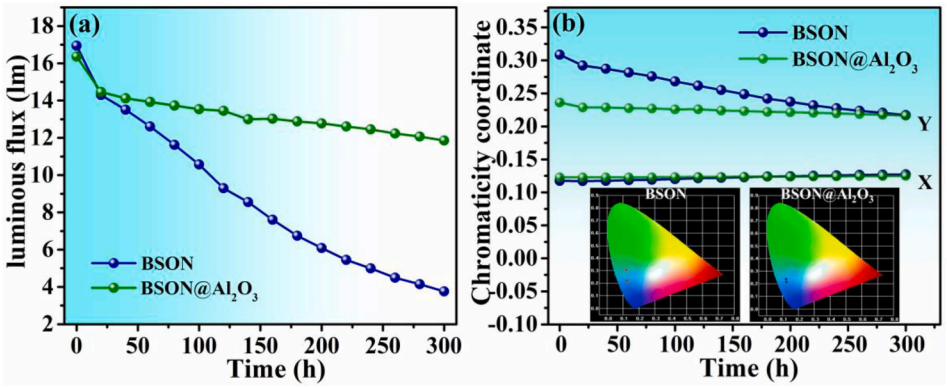

Fig. 7. Luminous flux (a) and chromaticity coordinates (b) of the LEDs fabricated with BSON and BSON@Al_2O_3 deposited for 20 cycles, as a function of the aging time.

fabricated using BSON@Al_2O_3, remaining 73% of the initial value. The LEDs using BSON@Al_2O_3 show a luminous flux of 3 times higher than those of the LEDs using the uncoated BSON after aging for 300 h. Simultaneously, the chromaticity coordinates of the cyan LEDs fabricated using BSON@Al_2O_3 nearly maintain unchanged with aging time (Fig. 7b). Therefore, it demonstrates that the Al_2O_3 protective layer enables to effectively improve the reliability of LEDs using the coated BSON phosphor.

4. Conclusions

In this work, the thermal degradation stability of the BSON phosphor was greatly enhanced by coating an ultra-thin Al_2O_3 layer on its surface through the FB-ALD technique. The coating thickness was precisely controlled by changing the cycles of deposition. The photoluminescence intensity and QE of BSON@Al_2O_3 slightly decreased as compared to those of the uncoated phosphor, while the oxidization resistance of the BSON@Al_2O_3 matrix was greatly improved. Under the moisture-assisted thermal treatment condition at 200 °C, the degradation of BSON was ascribed to the oxidation of both the host lattice and Eu^{2+}. On the other hand, the Al_2O_3 coating largely prevented the moisture-assisted thermal degradation of the phosphor. The cyan LEDs fabricated with BSON@Al_2O_3 showed considerably higher reliability, indicating the positive role of the ultra-thin Al_2O_3 layer prepared by the FB-ALD technique.

Declaration of competing interest

The authors declare that they have no known competing financial interests or personal relationships that could have appeared to influence the work reported in this paper.

Acknowledgments

This work was financially supported by the National Key Research and Development Program (MOST, Nos. 2022YFB350380 and 2022YFB3503801), and the National Natural Science Foundation of China (Nos. 52002120 and 51561135015). Yujie Zhao thanks the China Scholarship Council for supporting her to study ALD technique in the Netherlands. The authors would like to thank Mojgan Talebi for the experimental support.

References

[1] X.X. Sheng, P.P. Dai, Z.Y. Sun, D.W. Wen, Site-selective occupation of Eu^{2+} activators toward full-visible-spectrum emission in well-designed borophosphate phosphors, Chem. Eng. J. 395 (2020), 125141, https://doi.org/10.1016/j.cej.2020.125141.

[2] Z.Y. Yang, G.C. Liu, Y.F. Zhao, Y.Y. Zhou, J.W. Qiao, M.S. Molokeev, H.C. Swart, Z. G. Xia, Competitive site occupation toward improved quantum efficiency of $SrLaScO_4$:Eu red phosphors for warm white LEDs, Adv. Opt. Mater. 10 (2022), 2102373, https://doi.org/10.1002/adom.202102373.

[3] Y.H. Xu, L. Zhang, S.W. Yin, X.D. Wu, H.P. You, Highly efficient green-emitting phosphors with high color rendering for WLEDs, J. Alloys Compd. 911 (2022), 165149, https://doi.org/10.1016/j.jallcom.2022.165149.

[4] R. Shi, X.J. Zhang, Z.X. Qiu, J.L. Zhang, S.Z. Liao, W.L. Zhou, X.H. Xu, L.P. Yu, S. X. Lian, Composition and antithermal quenching of noninteger stoichiometric Eu^{2+}-doped Na-beta-Alumina with cyan emission for near-UV WLED, Inorg. Chem. 60 (2021) 19393–19401, https://doi.org/10.1021/acs.inorgchem.1c03220.

[5] Z.Y. Wu, C. Li, F. Zhang, S.X. Huang, F.J. Wang, X.M. Wang, H. Jiao, High-performance ultra-narrow-band green-emitting phosphor $LaMgAl_{11}O_{19}:Mn^{2+}$ for wide color-gamut WLED backlight displays, J. Mater. Chem. C 10 (2022) 7443–7448, https://doi.org/10.1039/d2tc00850e.

[6] J.M. Tang, J.Y. Si, G.H. Li, T.L. Zhou, Z.Z. Zhang, G.M. Cai, Excellent enhancement of thermal stability and quantum efficiency for $Na_2BaCa(PO_4)_2:Eu^{2+}$ phosphor based on Sr doping into Ca, J. Alloys Compd. 911 (2022), 165092, https://doi.org/10.1016/j.jallcom.2022.165092.

[7] J.W. Qiao, J. Zhao, Q.L. Liu, Z.G. Xia, Recent advances in solid-state LED phosphors with thermally stable luminescence, J. Rare Earths 37 (2019) 565–572, https://doi.org/10.1016/j.jre.2018.11.001.

[8] Y.H. Wang, J.Y. Ding, Y.C. Wang, X.F. Zhou, Y.X. Cao, B. Ma, J.Y. Li, X.C. Wang, T. Seto, Z.Y. Zhao, Structural design of new Ce^{3+}/Eu^{2+}-doped or co-doped phosphors with excellent thermal stabilities for WLEDs, J. Mater. Chem. C 7 (2019) 1792–1820, https://doi.org/10.1039/c8tc06013d.

[9] J.H. Tian, W.D. Zhuang, Thermal stability of nitride phosphors for light-emitting diodes, Inorg. Chem. Front. 8 (2021) 4933–4954, https://doi.org/10.1039/d1qi00993a.

[10] D.C. Huang, H.M. Zhu, Z.H. Deng, Q.L. Zou, H.Y. Lu, X.D. Yi, W. Lu, C.Z. Guo, X. Y. Chen, Moisture-resistant Mn^4-doped core-shell-structured fluoride red phosphor exhibiting high luminous efficacy for warm white light-emitting diodes, Angew. Chem., Int. Ed. 58 (2018) 3843–3847, https://doi.org/10.1002/anie.201813363.

[11] J. Qiao, S. Zhang, X.Q. Zhou, W.B. Chen, R. Gautier, Z.G. Xia, Near-infrared light-emitting diode utilizing europium-activated calcium oxide phosphor with external quantum efficiency of up to 54.7, Adv. Mater. 34 (2022), 2201887, https://doi.org/10.1002/adma.202201887.

[12] Y.Q. Li, A.C.A. Delsing, G. de With, H.T. Hintzen, Luminescence properties of Eu^{2+}-activated alkaline-earth silicon-oxynitride $MSi_2O_{2-\delta}N_{2+2/3\delta}$ (M = Ca, Sr, Ba): a promising class of novel LED conversion phosphors, Chem. Mater. 17 (2005) 3242–3248, https://doi.org/10.1021/cm050175d.

[13] Y. Song, Y. Song, K. Toda, T. Masaki, D. Yoon, Synthesis and photoluminescence properties of oxynitride phosphors $M_{0.98}Si_2O_2N_2:Eu^{2+}_{0.02}$ (M = Ba, Sr, Ca) using the cellulose assisted liquid phase precursor process, Ceram. Int. 42 (2016) 9667–9672, https://doi.org/10.1016/j.ceramint.2016.03.055.

[14] G.G. Li, C.C. Lin, W.T. Chen, M.S. Molokeev, V.V. Atuchin, C.Y. Chiang, W.Z. Zhou, C.W. Wang, W.H. Li, H.S. Sheu, T.S. Chan, C.G. Ma, R.S. Liu, Photoluminescence tuning via cation substitution in oxonitridosilicate phosphors: DFT calculations, different site occupations, and luminescence mechanisms, Chem. Mater. 26 (2014) 2991–3001, https://doi.org/10.1021/cm500844v.

[15] Y.Q. Li, G. de With, H.T. Hintzen, Luminescence of a new class of UV-blue-emitting phosphors $MSi_2O_{2-\delta}N_{2+2/3\delta}:Ce^{3+}$ (M = Ca, Sr, Ba), J. Mater. Chem. 15 (2005) 4492–4496, https://doi.org/10.1039/b507735d.

[16] M. Zhang, X. He, J.Y. Luo, Q.G. Zeng, Dependence of optical properties on the composition of $(Ba_{1-x-y}S_{rx}Eu_y)Si_2O_2N_2$ phosphors for white light emitting diodes, Mater. Chem. Phys. 147 (2014) 968–973, https://doi.org/10.1016/j.matchemphys.2014.06.044.

[17] X. Min, M.Z. Hu, Y.Y. Yang, B.F. Liu, Y.H. Wu, Y.S. Wu, L.X. Yu, Effects of fluxes on preparation and luminescence properties of $CaSi_2O_2N_2$: Eu^{2+} phosphors, Opt. Mater. 117 (2021), 111203, https://doi.org/10.1016/j.optmat.2021.111203.

[18] N. Kimura, K. Sakuma, S. Hirafune, K. Asano, N. Hirosaki, R.-J. Xie, Extrahigh color rendering white light-emitting diode lamps using oxynitride and nitride phosphors excited by blue light-emitting diode, Appl. Phys. Lett. 90 (2007), 051109, https://doi.org/10.1063/1.2437090.

[19] Y.H. Gu, Q.H. Zhang, Y.G. Li, H.Z. Wang, Nitridation from core-shell oxides for tunable luminescence of $BaSi_2O_2N_2:Eu^{2+}$ LED phosphors, J. Mater. Chem. 20 (2010) 6050–6056, https://doi.org/10.1039/c0jm00118j.

[20] B.-G. Yun, T. Horikawa, H. Hanzawa, K.-i. Machida, Preparation and luminescence properties of single-phase $BaSi_2O_2N_2:Eu^{2+}$, a bluish-green phosphor for white light-emitting diodes, J. Electrochem. Soc. 157 (2010) J364–J370, https://doi.org/10.1149/1.3479763.

[21] H.H. Wang, Z.H. Zhu, B.L. Ma, L.S. Wei, L.K. Li, Improved thermal stability and luminescence properties of $SrSi_2O_2N_2:Eu^{2+}$ green phosphor by a heterogeneous precipitation protocol for solid-state lighting applications, Ceram. Int. 47 (2021) 24163–24169, https://doi.org/10.1016/j.ceramint.2021.05.127.

[22] J.S. Huo, W. Lu, B.Q. Shao, Y. Song, Y. Feng, S. Zhao, H. You, Enhanced luminescence intensity of $CaSi_2O_2N_2$: Eu^{2+} phosphor by using flux in the preparation process and incorporating Gd^{3+} ions, J. Lumin. 180 (2016) 46–50, https://doi.org/10.1016/j.jlumin.2016.08.014.

[23] C.-Y. Wang, R.-J. Xie, F. Li, X. Xu, Thermal degradation of the green-emitting $SrSi_2O_2N_2:Eu^{2+}$ phosphor for solid state lighting, J. Mater. Chem. C 2 (2014) 2735–2742, https://doi.org/10.1039/c3tc32582b.

[24] H. Zhang, Z.Y. Cheng, Y.J. Zhang, Z.Q. Hu, J.J. Yu, N.Y. Zou, Improved luminescence properties and thermal stability of $SrSi_2O_2N_2:Eu^{2+}$ phosphor with single phase via the formation of Eu^{3+} on surface structure, J. Mater. Sci. 52 (2017) 7605–7614, https://doi.org/10.1007/s10853-017-0992-y.

[25] D. Wu, L.L. Liu, H.B. Duan, J.R. Wang, W.F. Zou, J.Q. Peng, X.Y. Ye, A comparison research on replacements of Ba^{2+} by Lu^{3+} and Ba^{2+}-Si^{4+} by Lu^{3+}-Al^{3+} in $BaSi_2O_2N_2$:Eu phosphors, J. Rare Earths 40 (2022) 20–28, https://doi.org/10.1016/j.jre.2021.07.006.

[26] L.L. Wang, H.Y. Ni, Q.H. Zhang, F.M. Xiao, Research on the luminescence and temperature quenching properties of $BaSi_2O_2N_2:Eu^{2+}$ phosphor, J. Nanosci. Nanotechnol. 16 (2016) 4008–4011, https://doi.org/10.1166/jnn.2016.11839.

[27] J.S. Huang, R.H. Liu, B. Hu, Effect of fluxes on synthesis and luminescence properties of $BaSi_2O_2N_2:Eu^{2+}$ oxynitride phosphors, J. Rare Earths 36 (2018) 225–230, https://doi.org/10.1016/j.jre.2017.07.005.

[28] D. Wu, L. Fu, S.A. He, F.F. Xu, L.L. Liu, L.Q. Yao, F. Du, J.Q. Peng, X.Y. Ye, Significantly enhanced luminescence efficiency and thermal stability of $BaSi_2O_2N_2:Eu^{2+}$ phosphor by doping a very small amount of SiC, Ceram. Int. 46 (2020) 25382–25391, https://doi.org/10.1016/j.ceramint.2020.07.006.

[29] Y.P. Zhang, X.C. Chen, Y.B. Fu, C. Liang, Improving the thermal properties of $BaSi_2O_2N_2:Eu^{2+}$ phosphor by SiO_2 coating, J. Synth. Cryst. 48 (2019) 1247–1253, https://doi.org/10.16553/j.cnki.issn1000-985x.2019.07.011.

[30] M. Zhao, K. Cao, M.J. Liu, J. Zhang, R. Chen, Q.Y. Zhang, Z.G. Xia, Dual-shelled $RbLi(Li_3SiO_4)_2:Eu^{2+}$@$Al_2O_3$@ODTMS phosphor as a stable green emitter for high-power LED Backlights, Angew. Chem., Int. Ed. 59 (2020) 12938–12943, https://doi.org/10.1002/anie.202003150.

[31] J. Xie, A.D. Sendek, E.D. Cubuk, X.K. Zhang, Z.Y. Lu, Y.J. Gong, T. Wu, F.F. Shi, W. Liu, E.J. Reed, Y. Cui, Atomic layer deposition of stable $LiAlF_4$ lithium ion conductive interfacial layer for stable cathode cycling, ACS Nano 11 (2017) 7019–7027, https://doi.org/10.1021/acsnano.7b02561.

[32] Y.J. Zhao, L.J. Yin, O.M. Ten Kate, B. Dierre, R. Abellon, R.-J. Xie, J.R. Van Ommen, H.T. Hintzen, Enhanced thermal degradation stability of the $Sr_2Si_5N_8:Eu^{2+}$ phosphor by ultra-thin Al_2O_3 coating through the atomic layer deposition technique in a fluidized bed reactor, J. Mater. Chem. C 7 (2019) 5772–5781, https://doi.org/10.1039/c9tc01063g.

[33] S.M. George, Atomic layer deposition: an overview, Chem. Rev. 110 (2009) 111–131, https://doi.org/10.1021/cr900056b.

[34] H. Van Bui, F. Grillo, J.R. Van Ommen, Atomic and molecular layer deposition: off the beaten track, Chem. Commun. 53 (2017) 45–71, https://doi.org/10.1039/c6cc05568k.

[35] V. Miikkulainen, M. Leskelä, M. Ritala, R.L. Puurunen, Crystallinity of inorganic films grown by atomic layer deposition: overview and general trends, J. Appl. Phys. 113 (2013) 2, https://doi.org/10.1063/1.4757907.

[36] R.L. Puurunen, Formation of metal oxide particles in atomic layer deposition during the chemisorption of metal chlorides: a review, Chem. Vap. Depos. 11 (2005) 79–90, https://doi.org/10.1002/chin.200518202.

[37] R.L. Puurunen, Surface chemistry of atomic layer deposition: a case study for the trimethylaluminum/water process, J. Appl. Phys. 97 (2005), 121301, https://doi.org/10.1063/1.1940727.

[38] N.M. Figueiredo, N.J.M. Carvalho, A. Cavaleiro, An XPS study of Au alloyed Al-O sputtered coatings, Appl. Surf. Sci. 257 (2011) 5793–5798, https://doi.org/10.1016/j.apsusc.2011.01.104.

[39] J. Guo, H. Van Bui, D. Valdesueiro, S.J. Yuan, B. Liang, J.R. Van Ommen, Suppressing the photocatalytic activity of TiO_2 nanoparticles by extremely thin Al_2O_3 films grown by gas-phase deposition at ambient conditions, Nanomaterials 8 (2018) 61, https://doi.org/10.3390/nano8020061.

[40] Y. Chen, F.J. Pan, M. Wang, X.J. Zhang, J. Wang, M.M. Wu, C.X. Wang, Blue-emitting phosphor $Ba_4OCl_6:Eu^{2+}$ with good thermal stability and a tiny chromaticity shift for white LEDs, J. Mater. Chem. C 4 (2016) 2367–2373, https://doi.org/10.1039/c5tc02806j.

[41] J. Zhu, L. Wang, T.L. Zhou, Y.J. Cho, T. Suehiro, T. Takeda, M. Lu, T. Sekiguchi, N. Hirosaki, R.-J. Xie, Moisture-induced degradation and its mechanism of (Sr,Ca)$AlSiN_3:Eu^{2+}$, a red-color-converter for solid state lighting, J. Mater. Chem. C 3 (2015) 3181–3188, https://doi.org/10.1039/c4tc02824d.

[42] A.C. Dillon, A.W. Ott, J.D. Way, S.M. George, Surface-chemistry of Al_2O_3 deposition using $Al(CH_3)_3$ and H_2O in A binary reaction sequence, Surf. Sci. 322 (1995) 230–242, https://doi.org/10.1016/0039-6028(95)90033-0.

[43] M.B.M. Mousa, C.J. Oldham, G.N. Parsons, Atmospheric pressure atomic layer deposition of Al_2O_3 using trimethyl aluminum and ozone, Langmuir 30 (2014) 3741–3748, https://doi.org/10.1021/la500796r.

[44] F.F. Yao, L. Wang, Y. Lv, Y.X. Zhuang, T.-L. Zhou, R.-J. Xie, Composition-dependent thermal degradation of red-emitting $(Ca_{1-x}Sr_x)AlSiN_3:Eu^{2+}$ phosphors for high color rendering white LEDs, J. Mater. Chem. C 6 (2018) 890–898, https://doi.org/10.1039/c7tc04356b.